Modeling Scattering from Rough Poroelastic Surfaces Using COMSOL Multiphysics

Anthony L. Bonomo[*1], Marcia J. Isakson[1], and Nicholas P. Chotiros[1]
[1]Applied Research Laboratories, The University of Texas, Austin, TX USA
*Corresponding author: 10,000 Burnet Road, Austin, TX 78758, abonomo@arlut.utexas.edu

Abstract: COMSOL Multiphysics is used to address the problem of acoustic scattering from one-dimensional rough poroelastic surfaces. The poroelastic sediment is modeled following the Biot-Stoll formulation. The rough surfaces are generated using a modified power law spectrum. Both monostatic and bistatic scattering strengths are calculated. These results are compared with more conventional scattering models such as perturbation theory and the small-slope approximation. The finite element method is found to be a useful way to assess the validity of these scattering models.

Keywords: Underwater acoustics, Biot theory, poroelasticity, rough surface scattering.

1. Introduction

Acoustic scattering from the seafloor can be a significant source of noise in sonar systems especially in shallow water [1]. For this reason, accurate models that describe both the physics of the sediment and the interaction of acoustic waves with the bottom are necessary. Seafloor roughness is of particular significance, as it can be a dominant contributor to sound scattering at higher acoustic frequencies.

The acoustic behavior of sediments has been studied extensively. The earliest models assumed sediments behaved like fluids. Since sediments generally can support shear stresses, the assumptions made when using fluid models are tenuous at best and have been replaced with more robust models, such as those that model the sediment as an elastic or viscoelastic material [1]. However, it has recently been shown that the best fit with experimental reflection data occurs when the sediment is assumed to behave as a poroelastic medium [2]. The theory of sound propagation in poroelastic media was first introduced by Biot in a series of classic papers [3]–[10]. This formulation was extended by Stoll and Kan and applied to the problem of wave reflection from a flat fluid-porous interface [11].

Much work has also been done toward quantifying the effects of surface roughness on the pressure field scattered from the seafloor. Scattering problems are typically studied using theoretical models that make various assumptions in approximating the Helmholtz-Kirchhoff integral. The three most common of these methods are the small-roughness perturbation approximation, the Kirchhoff approximation, and the small-slope approximation [1]. Recently, the small-roughness perturbation approximation and the small-slope approximation have been extended to scattering from rough poroelastic surfaces [12]-[13].

This work seeks to study the acoustic scattering from one-dimensional rough poroelastic surfaces using the finite element method. The monostatic and bistatic scattering strengths are calculated using COMSOL Multiphysics and compared with the values obtained using existing approximation methods.

2. Problem Description

2.1 Physical Domain

The problem being addressed involves a plane wave obliquely incident on a rough interface separating two semi-infinite half-spaces, as shown in Figure 1.

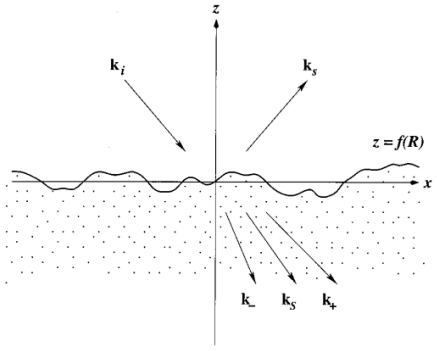

Figure 1. Geometry of scattering problem, as reproduced from [13].

The upper half-space consists of a fluid while the lower half-space is assumed to be a poroelastic medium. It is assumed that the lower medium is composed of two components: a solid elastic frame and an interstitial fluid. It is also assumed that the fluid of the upper medium is the same fluid as the interstitial fluid of the lower medium [13].

As shown in Figure 1, scattered and transmitted waves result when the incident plane wave impinges on the rough interface. The transmitted energy is distributed into three different waves—two compressional waves (denoted as the "fast" and "slow" waves) and a shear wave [11].

2.2 Equations of Motion

In the frequency domain, the equation governing the fluid half-space is the familiar Helmholtz equation with sound speed and density assumed to be constant, as shown below:

$$(\nabla^2 + k^2)p_a = 0, \tag{1}$$

where k is the wavenumber and p_a is the acoustic pressure.

A pair of coupled equations as developed by Biot describe the motion of the lower half-space. Again, if time-harmonic dependency is assumed, they are given as follows [9]:

$$-\rho_{av}\omega^2\mathbf{u} + \rho_f\omega^2\mathbf{w} - \nabla\cdot\sigma = 0 \tag{2}$$
$$-\rho_f\omega^2\mathbf{u} - \omega^2\rho_c(\omega)\mathbf{w} + \nabla p_f = 0, \tag{3}$$

where $\mathbf{u}$ is the displacement of the solid frame, σ is the total stress tensor, $\mathbf{w}$ is the fluid displacement with respect to the frame, ρ_f is the fluid density, and p_f is the fluid pore pressure. The complex density $\rho_c(\omega)$ is given by

$$\rho_c(\omega) = \frac{\tau}{\epsilon_p}\rho_f + \frac{\mu_f}{i\omega\kappa},$$

where τ is the tortuosity, ϵ_p is the porosity, μ_f is the fluid viscosity including Biot's high frequency correction, and κ is permeability. The average density $\rho_{av} = \rho_{dr} + \epsilon_p\rho_f$, where ρ_{dr} is the drained density.

For numerical calculations and ease of coupling with acoustic domains, it is often convenient to recast Eq. (2) and (3) in terms of the frame displacement $\mathbf{u}$ and the pore fluid pressure p_f [14]. Eq. (2) and (3) can thus be rewritten as follows [15]:

$$-\omega^2\left(\rho_{av} - \frac{\rho_f^2}{\rho_c(\omega)}\right)\mathbf{u} - \nabla\cdot\sigma = \frac{\rho_f}{\rho_c(\omega)}\nabla p_f \tag{4}$$
$$-\frac{\omega^2}{M}p_f + \nabla\cdot\frac{-1}{\rho_c(\omega)}\left(\nabla p_f - \omega^2\rho_f\mathbf{u}\right) = \omega^2\alpha_B\epsilon_{vol}, \tag{5}$$

where M is the Biot modulus, α_B is the Biot-Willis coefficient, and ϵ_{vol} is the volumetric strain.

2.3 Coupling Conditions

Assuming free flow across the interface, the conditions needed to couple an acoustic (fluid) domain to a poroelastic domain are given by the following equations [16]:

$$\sigma\hat{n} = -p_a\hat{n} \tag{6a}$$
$$\mathbf{u}\cdot\hat{n} + \mathbf{w}\cdot\hat{n} = \frac{1}{\rho_a\omega^2}\frac{\partial p_a}{\partial n} \tag{6b}$$
$$p_f = p_a. \tag{6c}$$

Equation (6a) ensures continuity of normal stresses. Equation (6b) enforces continuity of normal displacement. Equation (6c) invokes pressure continuity.

2.4 Rough Surface Characteristics

Random rough surfaces, like those found on the ocean bottom, are usually described statistically in terms of their deviation from a smooth reference surface [17]. One commonly used model assumes the seafloor roughness has a normalized spectral density, $W(K)$, described by a simple power law, where K is the spatial wavenumber [1]. While power law models have been found to agree closely with experimentally measured seafloor roughness in many cases, the fact that the power-law spectral form behaves pathologically when the spatial wavenumber approaches zero or infinity limits its utility. To address this issue, a modified power law spectrum is used in this work and is given by the following:

$$W(K) = \frac{A}{(K^2l^2+1)^2}, \tag{7}$$

where $A = 2h^2 l/\pi$. Here h is the *rms* surface height of the surface and l controls the spectral cutoff length [13]. It can easily be shown that the power spectrum described by Eq. (7) is equivalent to the more conventional von Karman power spectrum described in [1] and elsewhere.

3. Modeling Considerations

3.1 Model Geometry

Figure 2 depicts the problem geometry for a given rough surface realization as modeled in COMSOL. As shown, the rough surface separates a fluid domain from a domain assumed to consist of a poroelastic material. Both domains have height $2\lambda_a$ (as defined from the mean-plane of the rough interface), where λ_a is the acoustic wavelength. The length of the computational domain requires further consideration and is discussed in Section 3.3.

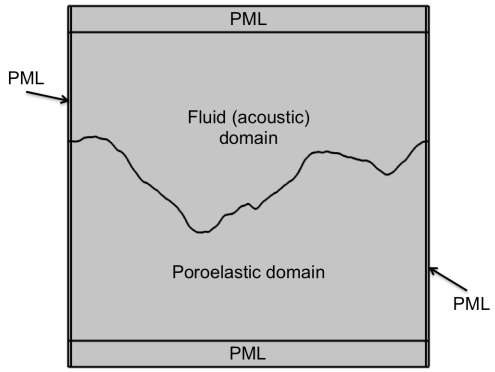

Figure 2. Model geometry.

In order to enforce the Sommerfeld radiation condition, perfectly matched layers (PMLs) are placed surrounding the entire computational domain. Rational coordinate stretching is selected for all PMLs. For PMLs adjacent to the acoustic domain, the expected wavelength is set to that of the compressional wave while for PMLs adjacent to the poroelastic domain, the expected wavelength is set to that of the so-called "fast" wave. All PMLs have thickness λ_a.

Each COMSOL model contains a rough surface realization generated following the procedure outlined in [18]. In short, for a given length L consisting of N points with spacing Δx, realizations following the chosen surface roughness spectral density are generated at points $x_n = n\Delta x\ (n = 1, \ldots, N)$ using the following expression:

$$f(x_n) = \frac{1}{L}\sum_{j=-N/2}^{N/2-1} F(K_j)\, e^{iK_j x_n}, \qquad (8)$$

where, for $j \geq 0$,

$$F(K_j) = \left[2\pi L W(K_j)\right]^{\frac{1}{2}} \begin{cases} \frac{[N(0,1)+iN(0,1)]}{\sqrt{2}}, & j \neq 0, \frac{N}{2} \\ N(0,1), & j = 0, \frac{N}{2} \end{cases},$$

for $j < 0$, $F(K_j) = F(K_{-j})^*$, and where $N(0,1)$ indicates an independent sample taken from a zero mean, unit variance Gaussian distribution and $K_j = 2\pi j/L$. Eq. (8) is implemented in MATLAB and, through LiveLink, the generated realization is used to create a rough surface in COMSOL by drawing and connecting a series of Bezier polygons. In general, twenty-five such COMSOL models with distinct rough surface realizations are created for any given parameter set.

3.2 Implementation of Required Physics

The two domains shown in Figure 2 are modeled using separate physics interfaces within COMSOL. The fluid domain is modeled using the Pressure Acoustics, Frequency Domain Interface and the entire domain and associated PMLs are defined as a Pressure Acoustics Model. Similarly, the poroelastic domain and associated PMLs are modeled using the Poroelastic Waves Interface and defined as a Poroelastic Material.

In order for the created COMSOL models to be physically accurate, the fluid and poroelastic domains must be coupled using the conditions described by Eq. (6). The continuity of normal stresses and the continuity of pressure are both enforced through a Porous, Pressure node in the Poroelastic Waves Interface. This node is assigned to the rough interface, and the pressure p_0 is set to the total acoustic pressure acting on the interface. A Normal Acceleration node in the Pressure Acoustics, Frequency Domain Interface is used to ensure continuity of normal displacements on the interface. Within the Normal Acceleration node, Inward Acceleration is selected as the type and a_n is set to

$-\omega^2(u_x\hat{n}_x + u_z\hat{n}_z)$, where u_x and u_z are the x- and z-components of the frame displacement field and $\hat{n}_x$ and $\hat{n}_z$ are the x- and z-components of the normal vector (pointing out from the poroelastic domain and into the fluid domain).

Two more node assignments are needed in the Pressure Acoustics, Frequency Domain Interface to complete the model. A Far-Field Calculation node is assigned to the rough interface since the far-field scattered pressure is needed to calculate the scattering strength (see Section 3.5). Finally, a Background Pressure Field node is assigned to the fluid domain (excluding PMLs) and a custom background pressure field is prescribed, as described in the next section.

3.3 Incident Wave

When modeling infinite domains, it is important to minimize scattering from the ends of surface realizations. This goal is accomplished by tapering incident plane waves such that they are of negligible strength when they reach the edge PMLs. For this work, a modified Gaussian taper function is applied to create an incident wave of the following form [18]:

$$p_i(\mathbf{r}) = \exp\left\{i\mathbf{k}_i \cdot \mathbf{r}[1 + w(\mathbf{r})] - \frac{(x - z\cot\theta)^2}{g^2}\right\}, \quad (9)$$

where

$$w(\mathbf{r}) = \frac{2(x - z\cot\theta)^2/g^2 - 1}{(kg\sin\theta)^2},$$

$\mathbf{k}_i$ is the incident wave vector, $\mathbf{r}$ is the position vector, θ is the mean grazing angle, k is the acoustic wavenumber, and g is a parameter that controls the beam waist.

For this work, a value of $g = L/4$ is used. In order to ensure that the modified Gaussian tapered plane wave accurately approximates a solution to the Helmholtz equation governing the fluid domain, the length of the computational domain must be chosen such that it obeys the Kapp criterion [19]:

$$L \geq \frac{4A\sqrt{2}}{k\theta\sin\theta}, \quad (10)$$

where a value of $A = 6.64$ is used in this work. In practice, the computational domain length is chosen such that $L = \max\left(\frac{4A\sqrt{2}}{k\theta\sin\theta}, 80\lambda_a\right)$. The incident wave is implemented in COMSOL by setting the user defined background pressure field p_b equal to $p_i(\mathbf{r})$ from Eq. (9).

3.4 Mesh Criteria

When attempting to resolve wave motion using quadratic shape functions, a good rule of thumb is to have elements be of uniform spacing and sized no larger than $\lambda/6$, where λ is the wavelength corresponding to the slowest wave in the medium. However, such a rule can lead to excessive computational cost for domains consisting of poroelastic materials, since the slow and shear waves can often be more than an order of magnitude less than the fast wave. Since both the slow and shear waves are quite lossy, a mesh that becomes gradually coarser as it gets further from the rough interface is sufficient for scattering calculations as long as the maximum element size does not exceed one-sixth of the fast wave's wavelength. It should be noted that for scattering from very rough surfaces, the rule of thumb stated above may be inadequate and a boundary layer may need to be implemented on the rough interface to properly resolve all components of the scattered pressure field.

3.5 Calculation of Scattering Strength

After a set of COMSOL models are run and the scattered pressure fields are solved for a given parameter set, the scattering cross section is calculated by using the following expression [18]:

$$\sigma_s(\theta, \theta_s) = \frac{\langle |p_s(\mathbf{r})|^2 \rangle r}{\sqrt{\pi/2}g\left[1 - 0.5(1 + 2\cot^2\theta)/(kg\sin\theta)^2\right]}, \quad (11)$$

where θ_s is the scattered angle and $\langle\ \rangle$ denotes ensemble averaging over all realizations. The scattering strength is then simply calculated as follows:

$$SS = 10\log\sigma_s(\theta, \theta_s)\,. \quad (12)$$

To calculate the monostatic scattering strengths, the scattered angle θ_s is set equal to the grazing angle θ and θ is swept from 0 to $\frac{\pi}{2}$. The bistatic scattering strengths are calculated by fixing θ and sweeping θ_s from 0 to π.

4. Results

Using the above procedure, monostatic and bistatic scattering strengths were calculated for a variety of parameter sets and compared with the results of more conventional scattering models. Both the surface roughness parameters and material properties considered were taken from [13] for ease of comparison with the perturbation theory and small-slope approximation results published by Yang et al. The calculated values were also compared with the Kirchhoff approximation calculated using both the Monte Carlo and formally averaged methods based on the discussion from [18] and [20]. Tables 1 and 2 show the material properties utilized and the parametric cases considered. As mentioned above, twenty-five surface realizations were generated for each parameter set and the calculated scattered pressure fields were formally averaged to obtain the scattering strengths. Results from two cases are presented in the sections below.

Table 1: Material properties.

Parameter	Values
Fluid sound speed (c_f)	1530 m/s
Fluid density (ρ_f)	1023 kg/m^3
Fluid compressibility (χ_f)	4.176×10^{-10} Pa^{-1}
Fluid viscosity (μ_f)	10^{-3} Pa·s
Drained density (ρ_d)	1404.5 kg/m^3
Drained bulk modulus (K)	43.6 + i2.08 MPa
Drained shear modulus (G)	29.2 + i3.86 MPa
Biot-Willis coefficient (α_B)	0.998–$i8.15\times10^{-5}$
Permeability (κ_p)	3×10^{-11} m^2
Tortuosity (τ)	1.2
Porosity (ϵ_p)	0.38
Reference frequency (f_c)	410.4 Hz

Table 2: Parameters studied.

Parameter	Values
Frequency (f)	100 Hz and 3 kHz
rms surface height (h)	0.1 and 1 m
Surface cutoff length (l)	10 m
Bistatic grazing angle (θ)	45 degrees

4.1 Monostatic Results

Figures 3 and 4 show the results for monostatic scattering strength. Figure 3 corresponds to the case of lowest surface roughness relative to the acoustic wavelength. It is clear from the figure that all scattering models show excellent agreement for this case. Note the deviation of the finite element model and Kirchhoff Monte Carlo results from the other scattering models at normal incidence. This disparity occurs because only the finite element and Kirchhoff Monte Carlo models account for the coherent effects in the specular direction, which corresponds to normal incidence when considering monostatic scattering.

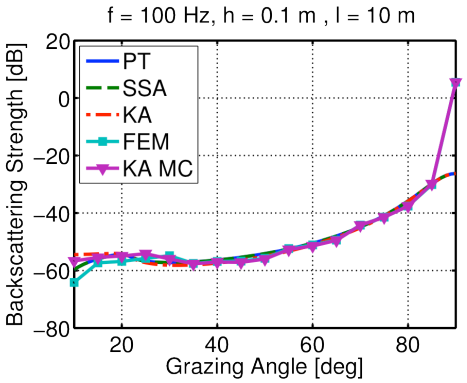

Figure 3. Monostatic scattering strengths for f = 100 Hz, h = 0.1 m, and l = 10 m.

Figure 4 corresponds to the case of highest surface roughness relative to the acoustic wavelength. All the scattering models show relatively good agreement for this case except for perturbation theory, which deviates significantly as the grazing angle approaches normal incidence. Also of note is the disparity between the finite element and small-slope approximation results for shallow grazing angles; the small-slope approximation is generally thought to perform best for cases like this one so this disparity warrants further study.

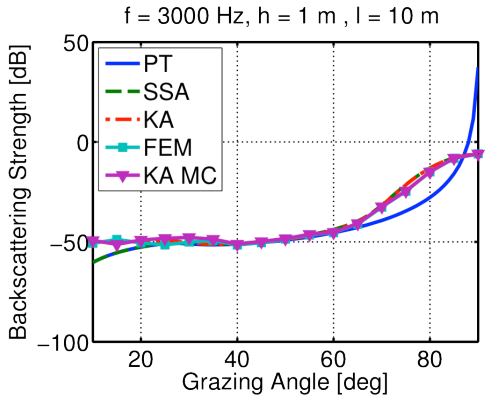

Figure 4. Monostatic scattering strengths for f = 3 kHz, h = 1 m, and l = 10 m.

4.2 Bistatic Results

Figures 5 and 6 show the results for bistatic scattering strength corresponding to a grazing angle of 45 degrees. Again, Figure 5 shows the case of lowest relative surface roughness. Like for the monostatic case, all scattering models shown have excellent agreement. The peak at 45 degrees shown by the finite element and Kirchhoff Monte Carlo results again represents the coherent specular contribution to the scattering, a feature not considered by the other models.

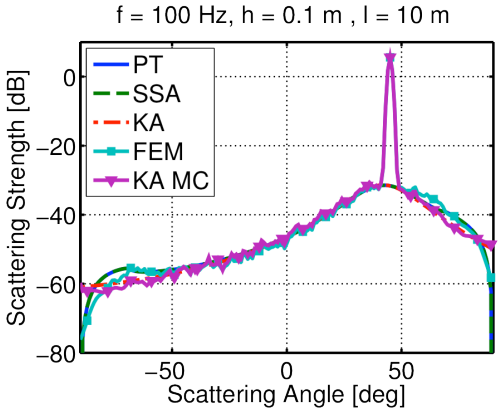

Figure 5. Bistatic scattering strengths for f = 10 Hz, h = 0.1 m, l = 10 m, and θ = 45°.

Like Figure 4, Figure 6 corresponds to the case of highest relative surface roughness. Here the finite element and small-slope approximation results agree very closely, while perturbation theory differs greatly at specular and both Kirchhoff methods deviate away from specular, as expected.

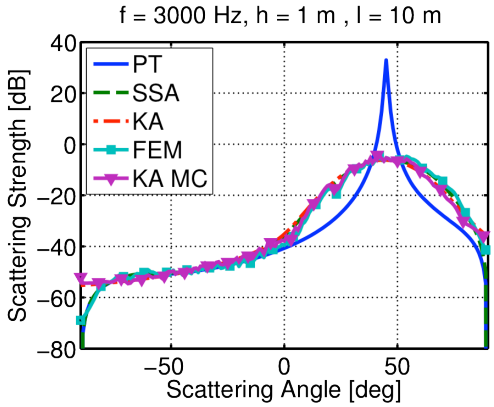

Figure 6. Bistatic scattering strengths for f = 3 kHz, h = 1 m, l = 10 m, and θ = 45°.

5. Conclusions and Future Work

The work presented here shows that COMSOL Multiphysics provides a robust way to solve scattering problems involving rough poroelastic surfaces and evaluate the efficacy of more conventional scattering models. In general, the finite element results agree very closely with those of the small-slope approximation. A small deviation was noted for the monostatic scattering at shallow grazing angles that should be investigated further. In the future, this work should be extended to scattering from two-dimensional surfaces and comparisons should be made between results from full poroelastic formulations and Biot-equivalent effective density fluid models, such as the one included in the Pressure Acoustics, Frequency Domain Interface.

6. References

1. D.R. Jackson & M.D. Richardson, *High-Frequency Seafloor Acoustics,* Springer, New York, NY (2007)

2. M.J Isakson, N.P Chotiros, R.A. Yarbrough, & J.N. Piper, "Quantifying the effects of roughness scattering on reflection loss measurements," *J. Acoust. Soc. Am.*, **132**(6), 3687-3697 (2012)

3. M.A. Biot, "Theory of elasticity and consolidation for a porous anisotropic solid," *J. App. Phys.*, **26**(2), 182-185 (1955)

4. M.A. Biot, "General solutions of the equations of elasticity and consolidation for a porous material," *J. App. Mech.*, **78**, 91-96 (1956)
5. M.A. Biot, "Theory of propagation of elastic waves in a fluid saturated porous solid. I. Low frequency range," *J. Acoust. Soc. Am.*, **28**(2), 168-178 (1956)
6. M.A. Biot, "Theory of propagation of elastic waves in a fluid saturated porous solid. I. High frequency range," *J. Acoust. Soc. Am.*, **28**(2), 179-191 (1956)
7. M.A. Biot, "Theory of deformation of a porous viscoelastic anisotropic solid," *J. App. Phys.*, **27**(5), 459-467 (1956)
8. M.A. Biot & D.G. Willis, "The elastic coefficients of the theory of consolidation," *J. App. Mech.*, **24**, 594-601 (1957)
9. M.A. Biot, "Mechanics of deformation and acoustic propagation in porous media," *J. App. Phys.*, **33**(4), 1482-1498 (1962)
10. M.A. Biot, "Generalized theory of acoustic propagation in porous dissipative media," *J. Acoust. Soc. Am.*, **34**(5), 1254-1264 (1962)
11. R.D. Stoll & T.K. Kan, "Reflection of acoustic waves at a water-sediment interface," *J. Acoust. Soc. Am.*, **70**(1), 149-156 (1981)
12. K.L Williams, J.M. Grochocinski, & D.R. Jackson, "Interface scattering by poroelastic seafloors: First-order theory," *J. Acoust. Soc. Am.*, **110**(6), 2956-2963 (2001)
13. T. Yang, S.L. Broschat, & C. Galea, "A comparison of perturbation theory and the small-slope approximation for acoustic scattering from a rough interface for a Biot medium," *IEEE J. Ocean Eng.*, **27**(3), 403-412 (2002)
14. N. Atalla, R. Panneton, & P. Debergue, "A mixed displacement-pressure formulation for poroelastic materials," *J. Acoust. Soc. Am.*, **104**(3), 1444-1452 (1998)
15. The COMSOL Group, "Theory for the Elastic Waves and Poroelastic Waves User Interfaces, *COMSOL Multiphysics v. 4.3b User's Guide*, 169-177 (2013)
16. H. Deresiewicz & R. Skalak, "On uniqueness in dynamic poroelasticity," *Bulletin of Seis. Soc. Am.*, **53**(4), 783-788 (1963)
17. J.A. Ogilvy, *Theory of Wave Scattering from Random Rough Surfaces,* IOP Publishing, Bristol, 9-29, (1992)
18. E.I. Thorsos, "The validity of the Kirchhoff approximation for rough surface scattering using a Gaussian roughness spectrum," *J. Acoust. Soc. Am.*, **83**(1), 78-92 (1988)
19. J. Toporkov, R.S. Awadallah, & G.S. Brown, "Issues relating to the use of a Gaussian-like incident field for low-grazing-angle scattering," *J. Opt. Soc. Am.*, **16**(1), 176-187 (1999)
20. E.I. Thorsos, "Acoustic scattering from a 'Pierson-Moskowitz' sea surface," *J. Acoust. Soc. Am.*, **88**(1), 78-92 (1990)

7. Acknowledgements

Thank you to the Office of Naval Research, Ocean Acoustics for financially supporting this work and to the American Society for Engineering Education for funding the lead author's SMART scholarship.